Available online at www.sciencedirect.com

ScienceDirect

Nuclear Physics B 960 (2020) 115166

NUCLEAR PHYSICS B

www.elsevier.com/locate/nuclphysb

Regular Bardeen AdS black hole as a heat engine

K.V. Rajani *, C.L. Ahmed Rizwan, A. Naveena Kumara, Deepak Vaid, K.M. Ajith

Department of Physics, National Institute of Technology Karnataka, Surathkal 575 025, India

Received 5 March 2020; received in revised form 25 July 2020; accepted 3 September 2020
Available online 11 September 2020
Editor: Stephan Stieberger

Abstract

We investigate the thermodynamic phase transition and heat engine efficiency in regular Bardeen AdS black hole. The thermodynamics of the black hole is analyzed in extended phase space. A first order phase transition analogous to van der Waal system is evident from this study, which is affirmed by the specific heat divergence at the critical points. A conventional heat engine is constructed by considering the black hole as working substance. The efficiency is obtained via a thermodynamic cycle in the $P - V$ plane, which receives and ejects heat. The heat engine efficiency is improved by adding a quintessence field. The analytical expression for heat engine efficiency is derived in terms of quintessence dark energy parameter.

1. Introduction

Black hole thermodynamics allows us to connect the quantum aspects of spacetime geometry with classical thermodynamic theory. The roots of this study trace back to the seminal work of Hawking and Bekenstein, where the temperature and entropy for a black hole were first defined [1–4]. It is natural to think that a system which possesses thermodynamic variables such as temperature and entropy should also satisfy the law of thermodynamics. Insisting that this should be true for black holes, Bardeen, Carter, and Hawking obtained the four laws of black hole thermo-

* Corresponding author.
E-mail addresses: rajanikv10@gmail.com (K.V. Rajani), ahmedrizwancl@gmail.com (C.L. Ahmed Rizwan), naviphysics@gmail.com (A. Naveena Kumara), dvaid79@gmail.com (D. Vaid), ajithkm@gmail.com (K.M. Ajith).

https://doi.org/10.1016/j.nuclphysb.2020.115166

dynamics [5]. A thermodynamic system can also exhibit various phases with different physical properties and phase transitions at certain critical values of the thermodynamic variables. This also turns out to be true for black holes as was first discovered by Hawking and Page in 1983 [6]. Interestingly enough this behavior is not observed for black holes in Minkowski spacetime, but instead for black holes in an asymptotically anti-deSitter (AdS) geometry. The reason for this is that one cannot define the microcanonical ensemble for a spacetime without a boundary.

Anti-deSitter spacetime entered the spotlight when Maldacena discovered the correspondence [7] between the *classical* bulk geometry of an AdS spacetime and a *quantum* conformal field theory living on the boundary of AdS. This "AdS/CFT" correspondence provided the first concrete construction of a quantum theory of gravity, or at the very least, a mapping between a quantum theory and a gravitational theory. Following Maldacena's discovery, the Hawking-Page transition - a first order phase transition between an AdS-Schwarzschild black hole and an AdS spacetime containing only thermal radiation was quickly understood to be the gravitational counterpart of the confinement-deconfinement phase transition in QCD [8].

Another milestone in black hole physics was the observation of a phase transition [9–11] in charged AdS black holes, similar to that seen in a van der Waals liquid-gas system. The original form of the first law of black hole thermodynamics is written by interpreting the mass of the black hole as the internal energy. For an electrically charged rotating black hole we have,

$$dM = TdS + \Omega dJ + \Phi dQ \tag{1}$$

where temperature T and entropy S are related to surface gravity κ and area of event horizon A respectively. Ω and J are the angular velocity and the momentum associated with rotation; Q and ϕ are the electric charge and potential. However, it was noticed that the black hole mass is more like the enthalpy H than internal energy U, which demands a thermodynamic variable in the black hole mechanics which can be interpreted as pressure [12]. The cosmological constant Λ was the natural candidate for thermodynamic pressure in AdS black holes for which the volume of the black hole V is conjugate quantity [13,14],

$$P = -\frac{\Lambda}{8\pi}. \tag{2}$$

The identification of cosmological constant as pressure in the first law made it consistent with Smarr formula. The extension of first law with PdV term lead to interesting developments in black hole thermodynamics. In particular, the thermodynamics of asymptotically AdS Reissner-Nordstrom black hole in the extended phase space exhibited rich phase structure analogous to van-der Waals (vdW) liquid-gas systems [15–17]. Since then, several studies were carried out in different AdS black holes in the extended phase space and the aforementioned similarity to vdW system is observed [18–23]. These first order phase transitions obey Maxwell's equal area law and Clausius-Clapeyron equations [24–28].

The recent developments in black hole thermodynamics are the Joule-Thomson (JT) expansion [29,30] and holographic heat engine in charged AdS black holes [31,32]. The holographic heat engines are basically traditional heat engines, but termed so by Clifford V. Johnson because their operation can be described by conformal field theories on the boundary [33]. Through this engine, a sufficient amount of mechanical work can be drawn from heat energy in AdS black holes. It is different from Penrose process in the rotating black holes, in which one can extract the rotational energy of the black hole from the ergosphere [34,35]. In the first holographic heat engine constructed by Johnson for charged AdS black hole, he calculated the efficiency of the

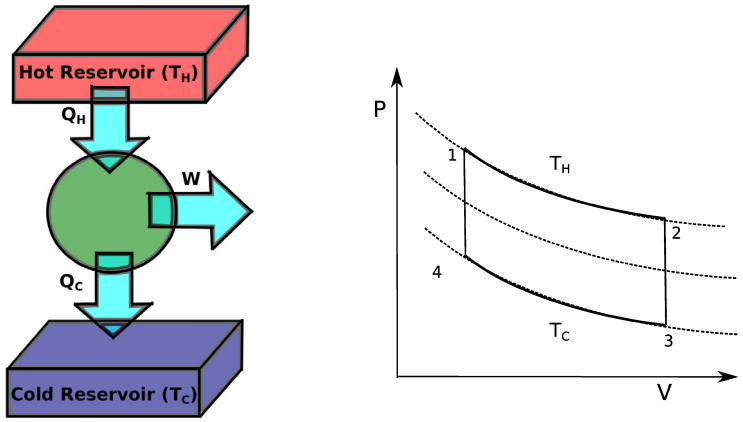

Fig. 1. The left figure is the schematic diagram of heat engine and right is Carnot engine cycle.

conversion. The idea of holographic heat engine is realized in various other contexts, static dyonic and dynamic black hole [36], polytropic black hole [37], Born-Infield black holes [38], $f(r)$ black holes [39], Gauss-Bonnet black holes [40], higher dimensional theories [25,41], massive black hole [42,43], in conformal gravity [44], in 3 dimensional charged BTZ black hole [45], in rotating black holes [46] and accelerating AdS black holes [47].

We would like to briefly introduce heat engines. A heat engine is constructed as a closed path in the $P-V$ plane, that absorbs Q_H amount of heat, and exhaust Q_C amount of heat (Fig. 1(a)). From the first law, the total mechanical work $W = Q_H - Q_C$. The efficiency of heat engine is given by,

$$\eta = \frac{W}{Q_H}. \tag{3}$$

The maximum possible efficiency for a heat engine is estimated from a Carnot engine, which is a theoretical thermodynamic cycle. The efficiency of Carnot engine is,

$$\eta_c = 1 - \frac{Q_C}{Q_H} = 1 - \frac{T_C}{T_H}, \tag{4}$$

where T_C and T_H are the lower and higher temperatures of the reservoir. This upper limit on efficiency is due to second law.

Now we construct a heat engine in the context of static black hole which has a simple heat cycle with a pair of isotherms at high temperature T_H and low temperature T_C Fig. 1(b). During isothermal expansion, Q_H amount of heat is being absorbed, and it will exhaust Q_C amount of heat during isothermal compression. We can connect these two temperatures by either isochoric paths as in Stirling cycle or adiabatic paths as in Carnot cycle, which is reversible. Entropy and volume for a static black hole are dependent on each other. So adiabats and isochores are alike, implies Carnot engine and Stirling engine are identical.

In Fig. 1(b) along the isotherm $1 \to 2$, the amount of heat absorbed,

$$Q_H = T_H\, \Delta S_{1\to 2} = T_H \left(\frac{3}{4\pi}\right)^{\frac{2}{3}} \pi \left(V_2^{\frac{2}{3}} - V_1^{\frac{2}{3}}\right). \tag{5}$$

Along the isotherm $3 \rightarrow 4$, the amount of heat rejected,

$$Q_C = T_C \, \Delta S_{3\rightarrow 4} = T_C \left(\frac{3}{4\pi}\right)^{\frac{2}{3}} \pi \left(V_3^{\frac{2}{3}} - V_4^{\frac{2}{3}}\right). \tag{6}$$

We choose isochores to connect those isotherms, i.e., $V_2 = V_3$ and $V_1 = V_4$. Then equations (5) and (6) lead to,

$$\eta = 1 - \frac{Q_C}{Q_H} = 1 - \frac{T_C}{T_H}, \tag{7}$$

which is same as the efficiency of the Carnot engine [48].

In this paper, we extend Johnson's work to regular Bardeen AdS black hole. A regular black hole has no singularity at the origin and possesses an event horizon, the first of this kind was constructed by Bardeen in 1968 [49]. The charged version of Bardeen black hole is constructed by Ayon-Beato and Garcia as magnetic solutions to Einsteins equation coupled to nonlinear electrodynamics [50]. A charge free Bardeen solution was found by Hayward [51] in 2006. Among the several studies in the physics of regular black holes, the thermodynamics of regular Bardeen black hole is also investigated [52–54].

This paper is organized as follows. In section 2 we discuss the thermodynamics of regular Bardeen black hole, which is followed by the heat engine model in section 3. In section 4 the effect of quintessence on the efficiency is studied. The paper ends with results and discussions which is presented in section 5.

2. Thermodynamics of regular Bardeen black hole

The action for regular black hole solution coupled with nonlinear electrodynamics in AdS spacetime read as [50],

$$S = \int d^4x\sqrt{-g}\left(\frac{1}{16\pi}R + \frac{3}{8\pi l^2} - \frac{1}{4\pi}\mathcal{L}(\mathcal{F})\right). \tag{8}$$

Where R is the Einstein scalar, l the AdS radius and $\mathcal{L}(\mathcal{F})$ is the Lagrangian density corresponding to nonlinear electrodynamics source,

$$\mathcal{L}(\mathcal{F}) = \frac{3M}{\beta^3}\left(\frac{\sqrt{4\beta^2\mathcal{F}}}{1+\sqrt{4\beta^2\mathcal{F}}}\right)^{5/2}, \tag{9}$$

where $\mathcal{F} = F_{\mu\nu}F^{\mu\nu}$ is the electromagnetic field strength. The spherically symmetric solution for the above action has the form [53–55],

$$ds^2 = -f(r)dt^2 + \frac{dr^2}{f(r)} + r^2d\theta^2 + r^2\sin^2\theta d\phi^2, \tag{10}$$

where $f(r) = 1 - \frac{2\mathcal{M}(r)}{r} - \frac{\Lambda r^2}{3}$ and $\mathcal{M}(r) = \frac{Mr^3}{(r^2+\beta^2)^{3/2}}$. β is the monopole charge, M is the mass of the black hole, Λ is the cosmological constant given by $-\frac{3}{\ell^2}$. The event horizon of the black hole is articulated by $f(r_h) = 0$, which gives the black hole mass,

$$M = -\frac{\left(\beta^2 + r_h^2\right)^{3/2}\left(-8\pi P r_h^2 - 3\right)}{6r_h^2}. \tag{11}$$

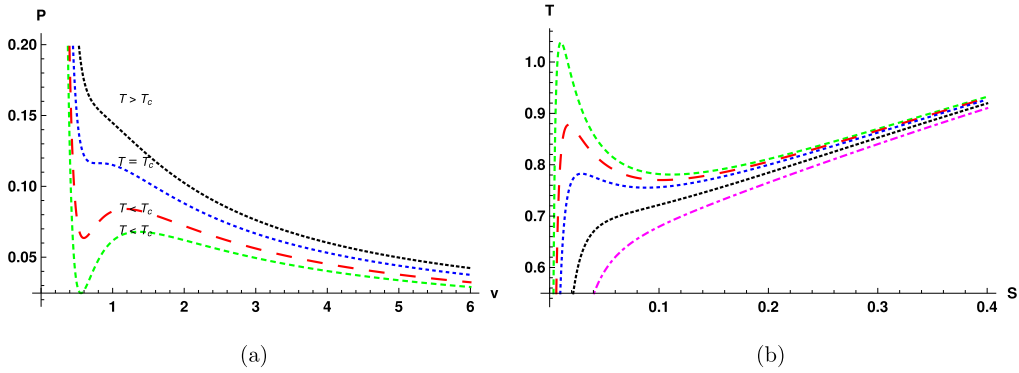

(a) (b)

Fig. 2. $P-v$ diagram for regular AdS black hole for different values of temperature with $\beta = 0.1$ (Fig. 2(a)). In Fig. 2(b) $T-S$ plot for different values of β is shown.

Now the first law of thermodynamics equation (1) can be rewritten as,

$$dM = TdS + VdP + \Psi d\beta. \tag{12}$$

Hawking temperature T can be obtained from surface gravity κ as,

$$T = \frac{\kappa}{2\pi} = \frac{1}{4\pi} f'(r)|_{r=r_h} = \frac{-2\beta^2 + 8\pi P r_h^4 + r_h^2}{4\pi r_h \left(\beta^2 + r_h^2\right)}. \tag{13}$$

The thermodynamic volume V and the entropy S can be derived from the first law (12) as,

$$V = \left.\frac{\partial M}{\partial P}\right|_{V,\beta} = \frac{4}{3}\pi r_h^3 \left(\frac{\beta^2}{r_h^2} + 1\right)^{3/2}, \tag{14}$$

$$S = \int \frac{dM}{T} = \pi r_h^2 \left(\left(1 - \frac{2\beta^2}{r_h^2}\right)\sqrt{\frac{\beta^2}{r_h^2} + 1} + \frac{3\beta^2 \log\left(\sqrt{\beta^2 + r_h^2} + r_h\right)}{r_h^2} \right). \tag{15}$$

The thermodynamic quantities depend on charge β explicitly. In the large r limit the entropy of Bardeen-AdS black hole is πr_h^2. Rearranging the equation (13) and identifying $v = 2r_h$ as specific volume, we obtain the equation of state $P(T, v, \beta)$,

$$P = \frac{2\pi T v \left(4\beta^2 + v^2\right) + 8\beta^2 - v^2}{2\pi v^4}. \tag{16}$$

We plot the $P-v$ isotherm and $T-S$ curves using the equations (13) and (16) as shown in Fig. 2. The behavior of $P-v$ diagram resembles that of van der Waals gas. The isotherm corresponding to $T = T_C$, called critical isotherm has an inflection point below which a critical behavior is displayed. The corresponding pressure and volume at that point are called critical pressure (P_C) and critical volume (v_C), respectively. The isotherms above critical point (for $T > T_C$) gradually approach equilateral hyperbolas, which corresponds to ideal gas case. On the other hand, the lower set of isotherms (for $T < T_C$) have the positive slope region ($\partial P/\partial v > 0$) which is thermodynamically unstable. The critical behavior is also apparent in $T-S$ plot.

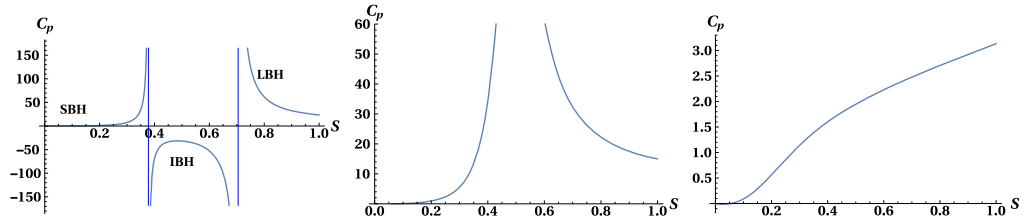

(a) (b) (c)

Fig. 3. Specific heat versus entropy diagram for regular AdS black hole with $\beta = 0.1$, for $P < P_c$ in Fig. 3(a), for $P = P_c$ in Fig. 3(b) and for $P > P_c$ in Fig. 3(c).

The critical point is characterized by the conditions,

$$\frac{\partial P}{\partial v} = 0 \quad , \qquad \frac{\partial^2 P}{\partial v^2} = 0. \tag{17}$$

The critical parameters hence obtained are,

$$v_c = \sqrt{2\left(\sqrt{273}+15\right)}\beta \quad , \quad T_c = -\frac{\left(\sqrt{273}-17\right)\sqrt{\frac{1}{2}\left(\sqrt{273}+15\right)}}{24\pi\beta} \quad , \tag{18}$$
$$P_c = \frac{\sqrt{273}+27}{12\left(\sqrt{273}+15\right)^2\pi\beta^2}.$$

We can compute $\frac{P_c v_c}{T_c}$ ratio,

$$\frac{P_c v_c}{T_c} = 0.367, \tag{19}$$

which almost matches with that of the van der Waals gas, which is 3/8.

One of the important physical quantities in thermodynamics is heat capacity. It is customary to define heat capacity in two different ways for a given system, i.e., at constant volume and at constant pressure. It is straightforward to show the following result,

$$C_V = T\left(\frac{\partial S}{\partial T}\right)_V = 0. \tag{20}$$

The heat capacity at constant pressure in the large r limit is obtained as

$$C_P = T\left(\frac{\partial S}{\partial T}\right)_P = \frac{2S\left(\pi\beta^2+S\right)\left(-2\pi\beta^2+8PS^2+S\right)}{2\pi^2\beta^4+\pi\beta^2S(24PS+7)+S^2(8PS-1)}. \tag{21}$$

The first order phase transition for the black hole is confirmed from the $C_P - S$ plot (Fig. 3). The critical behavior is seen only below certain pressure (P_c). There exist three distinct regions, and hence two divergence points for $P < P_C$. The positive specific heat for small black hole region (SBH) and large black hole region (LBH) means that those black holes are thermodynamically stable. Having negative specific heat, intermediate black hole region (IBH) represents unstable system. Therefore the actual phase transition takes place between SBH and LBH. The unstable region disappears at pressure $P = P_C$ resulting in a single divergence point.

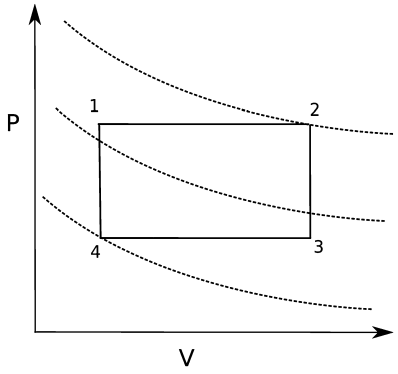

Fig. 4. Heat engine cycle.

3. Regular black hole as a heat engine

In this section, we calculate the efficiency of the heat engine constructed by taking regular Bardeen AdS black hole as working substance. As shown in Fig. 4, the new engine consists two isobars and two isochores/adiabats. For simplicity, we consider a rectangular cycle ($1 \to 2 \to 3 \to 4 \to 1$) in the $P - V$ plane. The area of the rectangle gives the work done, which reads

$$W = \oint P dV. \tag{22}$$

The total work done during one complete cycle,

$$W_{tot} = W_{1\to 2} + W_{3\to 4} = P_1(V_2 - V_1) + P_4(V_4 - V_3) \tag{23}$$

$$= \frac{4(P_1 - P_4)\left(\left(\pi\beta^2 + S_2\right)^{3/2} - \left(\pi\beta^2 + S_1\right)^{3/2}\right)}{3\sqrt{\pi}}. \tag{24}$$

As the heat capacity at constant volume, $C_V = 0$ one can conclude that no heat exchange takes place in the isochoric process. Therefore we calculate only heat absorbed Q_H during the process $1 \to 2$,

$$Q_H = \int_{T_1}^{T_2} C_P(P_1, T) dT = \int_{S_1}^{S_2} C_P \left(\frac{\partial T}{\partial S}\right) dS = \int_{S_1}^{S_2} T dS = M_2 - M_1, \tag{25}$$

$$= \frac{\left(\pi\beta^2 + S_2\right)^{3/2}(8P_1S_2 + 3)}{6\sqrt{\pi}S_2} - \frac{\left(\pi\beta^2 + S_1\right)^{3/2}(8P_1S_1 + 3)}{6\sqrt{\pi}S_1}. \tag{26}$$

Therefore efficiency of the engine is given by,

$$\eta = \frac{W}{Q_H} = \frac{8(P_1 - P_4)\left(\left(\pi\beta^2 + S_2\right)^{3/2} - \left(\pi\beta^2 + S_1\right)^{3/2}\right)}{\frac{\left(\pi\beta^2+S_2\right)^{3/2}(8P_1S_2+3)}{S_2} - \frac{\left(\pi\beta^2+S_1\right)^{3/2}(8P_1S_1+3)}{S_1}}. \tag{27}$$

The efficiency η can be compared with that of Carnot engine, η_C, which is the maximum possible efficiency. We take the higher temperature T_H as T_2 and lower temperature T_C as T_4 in equation (4). Then efficiency of Carnot engine is

$$\eta_C = 1 - \frac{\sqrt{S_2}\left(\pi\beta^2 + S_2\right)\left(-2\pi\beta^2 + 8P_4S_1^2 + S_1\right)}{\sqrt{S_1}\left(\pi\beta^2 + S_1\right)\left(-2\pi\beta^2 + 8P_1S_2^2 + S_2\right)}. \tag{28}$$

The efficiency η and the ratio η/η_C are plotted against entropy S_2 using the equations (27) and (28). As we can see in Fig. 5(a) the heat engine efficiency monotonously increases with S_2 (corresponding volume V_2) for all values of β, which implies that the increase in volume difference between small black hole (V_1) and large black hole (V_2) increases the efficiency. However this trend does not continue forever as the efficiency reaches saturation values after certain value of S_2. The dependence on charge β also visible from the same figure; the rates of increment are different for different β values. The plot η/η_C versus S_2 in Fig. 5(b) is consistent with second law, as it is bounded below 1. With the increase in charge β the ratio decreases. We also investigate the dependence of efficiency η on pressure P_1, the pressure at the source, which is shown in Fig. 5(c) and 5(d). Those two figures clearly show that the efficiency of the engine will approach the maximum possible value as the pressure approaches infinity. Before concluding this section we also mention that the monopole charge β has a positive effect on efficiency, i.e., higher the charge higher is the efficiency (Fig. 5(e), 5(f)).

4. Influence of quintessence on efficiency of heat engine

Following the work of Hang Liu and Meng, we study the effect of dark energy on thermodynamics and heat engine efficiency of regular black holes [48]. Quintessence is one of the candidates for dark energy which leads to accelerated expansion of the universe [56,57]. The real scalar field acts as a cosmic source having equation of state $p_q = \omega_q \rho_q$ $(-1 < \omega_q < -1/3)$. The density of quintessence field is given by,

$$\rho_q = -\frac{a}{2}\frac{3\omega_q}{r^{3(\omega_q+1)}}. \tag{29}$$

Kiselev was the first one to study effects of quintessence on a black hole [56]. Since then there were many studies in black holes surrounded by quintessence, to mention few, in the contexts of gauge gravity duality [58] and quasi normal modes [59]. Phase transitions in Reissner-Nordström and regular black holes with this exotic field were also studied [60–65]. When we include quintessence term in the metric of regular Bardeen AdS black hole, $f(r)$ is modified to

$$f(r) = 1 - \frac{2Mr^2}{\left(\beta^2 + r^2\right)^{3/2}} - \frac{a}{r^{3\omega_q+1}} - \frac{\Lambda r^2}{3}. \tag{30}$$

Where a is the normalization constant or strength parameter related to quintessence density and ω_q is the state parameter [53]. Now we proceed as in the earlier sections to obtain an expression for efficiency of the engine. Using the defining condition of event horizon, $f(r_h) = 0$, one can calculate the black hole mass as,

$$M = -\frac{1}{6}\left(\beta^2 + r_h^2\right)^{3/2} r^{-3(\omega_q+1)}\left(3a + \left(-8\pi P r_h^2 - 3\right) r_h^{3\omega_q+1}\right). \tag{31}$$

We can write the expression for temperature as,

$$T = \frac{r_h^{-3\omega_q-2}\left(3a\left(\beta^2(\omega_q+1) + r_h^2\omega_q\right) + r_h^{3\omega_q+1}\left(-2\beta^2 + 8\pi P r_h^4 + r_h^2\right)\right)}{4\pi\left(\beta^2 + r_h^2\right)}. \tag{32}$$

The heat capacity at constant pressure is,

$$C_P = \frac{2S\left(\pi\beta^2+S\right)\left(3a\pi^{\frac{3\omega_q+1}{2}}\left(\pi\beta^2(\omega_q+1)+S\omega_q\right)+S^{\frac{3\omega_q+1}{2}}\left(-2\pi\beta^2+8PS^2+S\right)\right)}{S^{\frac{3\omega_q+1}{2}}f_1(S)-3a\pi^{\frac{3\omega_q+1}{2}}f_2(S)}, \tag{33}$$

where,

$$f_1(S) = \left(2\pi^2\beta^4+\pi\beta^2S(24PS+7)+S^2(8PS-1)\right), \tag{34}$$

$$f_2(S) = \left(\pi^2\beta^4\left(3\omega_q^2+5\omega_q+2\right)+\pi\beta^2S\left(6\omega_q^2+7\omega_q+4\right)+S^2\omega_q(3\omega_q+2)\right). \tag{35}$$

Then we compute the heat Q_H along the process $1\to 2$ (the earlier arguments on no heat transfer for isochoric processes still hold),

$$\begin{aligned} Q_H &= \int_{T_1}^{T_2} C_P(P_1,T)dT = M_2 - M_1, \\ &= \frac{1}{6\sqrt{\pi}}\left\{\left(\pi\beta^2+S_1\right)^{3/2}S_1^{-\frac{3}{2}(\omega_q+1)}\left[3a\pi^{\frac{3\omega_q+1}{2}}-(8P_1S_1+3)S_1^{\frac{3\omega_q+1}{2}}\right]\right. \\ &\quad \left.+\left(\pi\beta^2+S_2\right)^{3/2}S_2^{-\frac{3}{2}(\omega_q+1)}\left[(8P_1S_2+3)S_2^{\frac{3\omega_q+1}{2}}-3a\pi^{\frac{3\omega_q+1}{2}}\right]\right\}. \end{aligned} \tag{36}$$

Having all the required quantities, the heat engine efficiency is expressed in terms of quintessence parameters a and ω_q as,

$$\eta = \frac{8(P_1-P_4)\left(\left(\pi\beta^2+S_2\right)^{3/2}-\left(\pi\beta^2+S_1\right)^{3/2}\right)}{f(S_1)+f(S_2)}, \tag{37}$$

where

$$f(S) = \left(\pi\beta^2+S\right)^{\frac{3}{2}}S^{-\frac{3}{2}(\omega_q+1)}\left[3a\pi^{\frac{3\omega_q}{2}+\frac{1}{2}}-(8P_1S+3)S^{\frac{3\omega_q}{2}+\frac{1}{2}}\right].$$

The efficiency of the Carnot engine is also obtained as earlier,

$$\eta_C = 1-\frac{\left(\pi\beta^2+S_2\right)S_1^{-\frac{3\omega_q}{2}-1}S_2^{\frac{3\omega_q}{2}+1}g(S_1,P_4)}{\left(\pi\beta^2+S_1\right)g(S_2,P_1)}, \tag{38}$$

where,

$$g(S,P) = \left(3a\pi^{\frac{3\omega_q}{2}+\frac{1}{2}}\left(\pi\beta^2(\omega_q+1)+S\omega_q\right)+S^{\frac{3\omega_q}{2}+\frac{1}{2}}\left(-2\pi\beta^2+8PS^2+S\right)\right).$$

The heat engine efficiency depends on pressure P, entropy S, monopole charge β and quintessence parameters a and ω_q. The above expressions reduce to the previous case when quintessence parameters $a=0$ and $\omega_q=0$. There is a significant increment in the efficiency against S_2 when we increase the quintessence strength a with other parameters being fixed (Fig. 6(a)). This change is visible in the ratio plot also (Fig. 6(b)). The plot for efficiency versus S_2 for different values of ω_q shows similar functional behavior in Fig. 6(c) and 6(d). But there is a difference in the physical effect, higher values of ω_q lead to smaller efficiency. With $\omega_q=-1$, black hole shows higher efficiency than $\omega_q=-1/3$ case, where efficiency takes a constant value

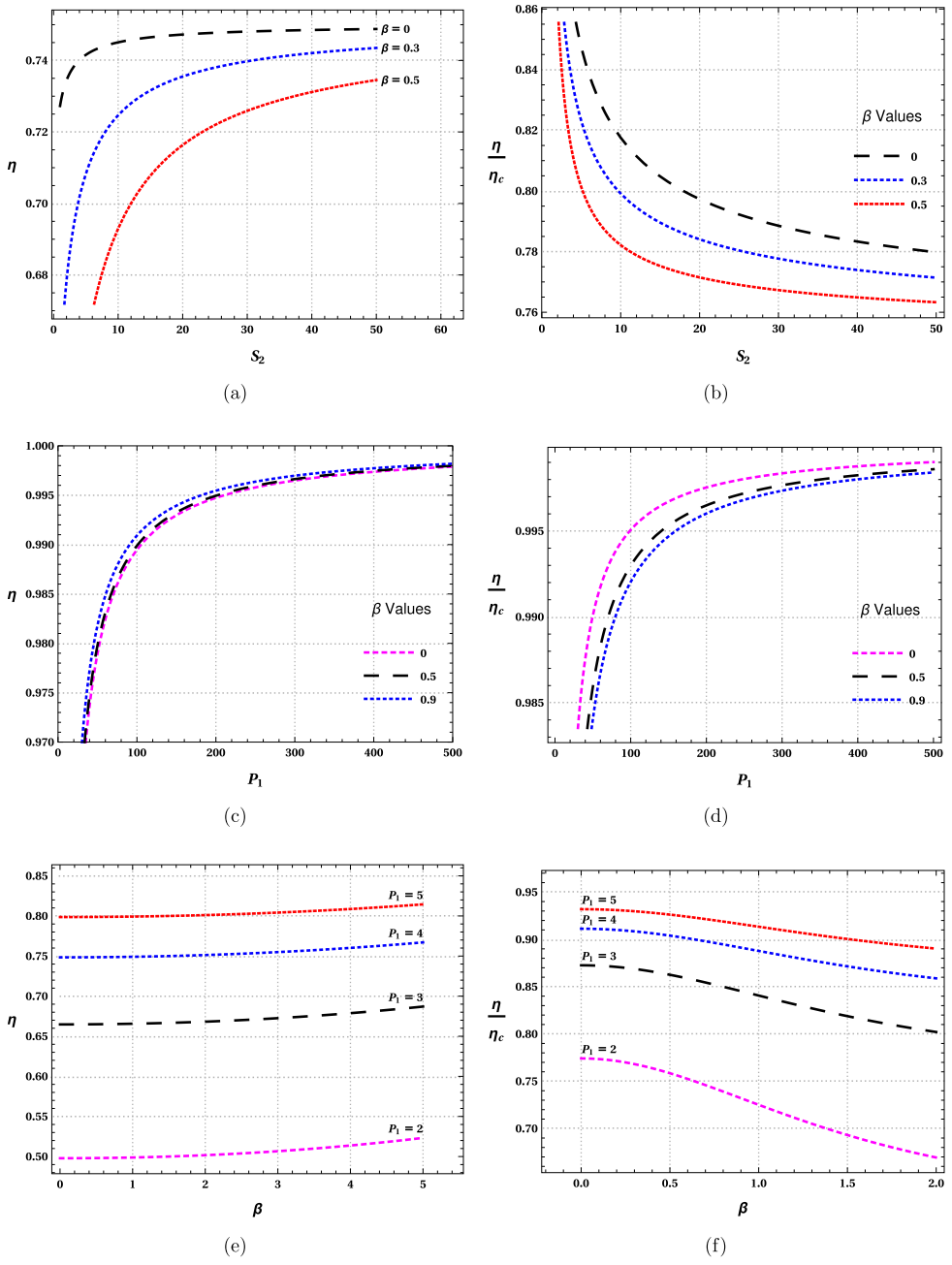

Fig. 5. *The variation of efficiency η of the engine with regular Bardeen black hole as the working substance and the ratio η/η_c with different variables.* In Fig. 5(a) and 5(b) the entropy dependence is shown with different values of β. Here we take $P_1 = 4$, $P_4 = 1$ and $S_1 = 1$. In the second set of Figs. 5(c) and 5(d) the variation with pressure is studied with different values of β. In this case we take $P_4 = 1$, $S_2 = 4$ and $S_1 = 1$. In the last set Fig. 5(e) and 5(f) the behavior against charge β with different values of P_1 is displayed. Here we take $S_2 = 20$, $P_4 = 1$ and $S_1 = 10$. The parameters P_1, P_4, S_1 and S_4 are chosen accordingly for the proper display of the nature of the plots.

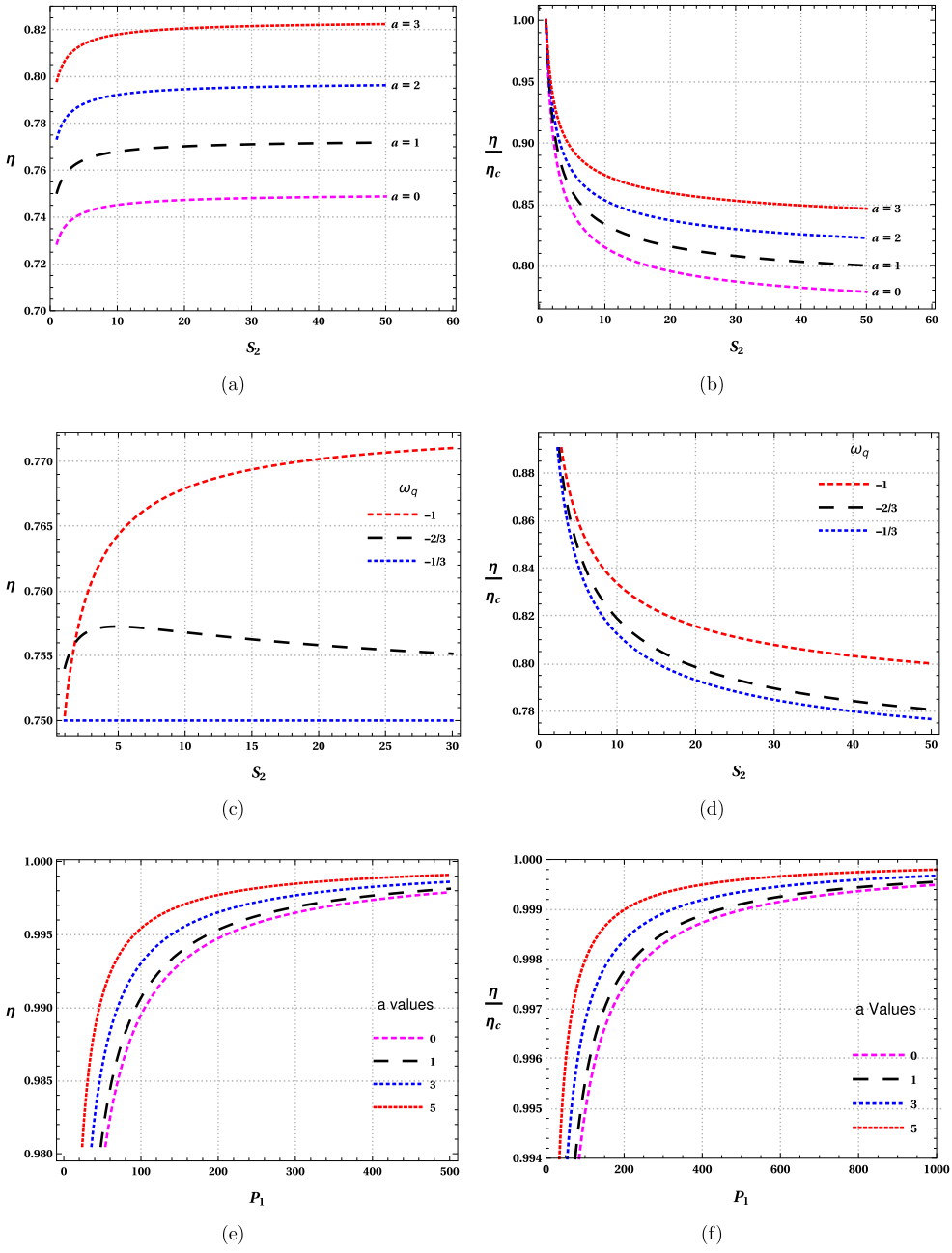

Fig. 6. *The effect of quintessence on the efficiency η of the engine and on the ratio η/η_c with different variables.* In the first set of Figs. 6(a) and 6(b) the variation with entropy is displayed with different values of a. Here we take $P_1 = 4$, $P_4 = 1$ $S_1 = 1$, $\omega_q = -1$ and $\beta = 0.1$. In the second set of Figs. 6(c) and 6(d) the variation with entropy for different values of ω_q is shown. In this case we take $P_1 = 4$, $P_4 = 1$ $S_1 = 1$, $a = 1$ and $\beta = 0.1$. In the last set 6(e) and 6(f) dependence on pressure for different values of a is observed with $P_4 = 1$ $S_1 = 1$, $S_2 = 4$, $\omega_q = -1$ and $\beta = 0.1$. Here also the fixed parameters are chosen appropriately for the proper observation of the effect.

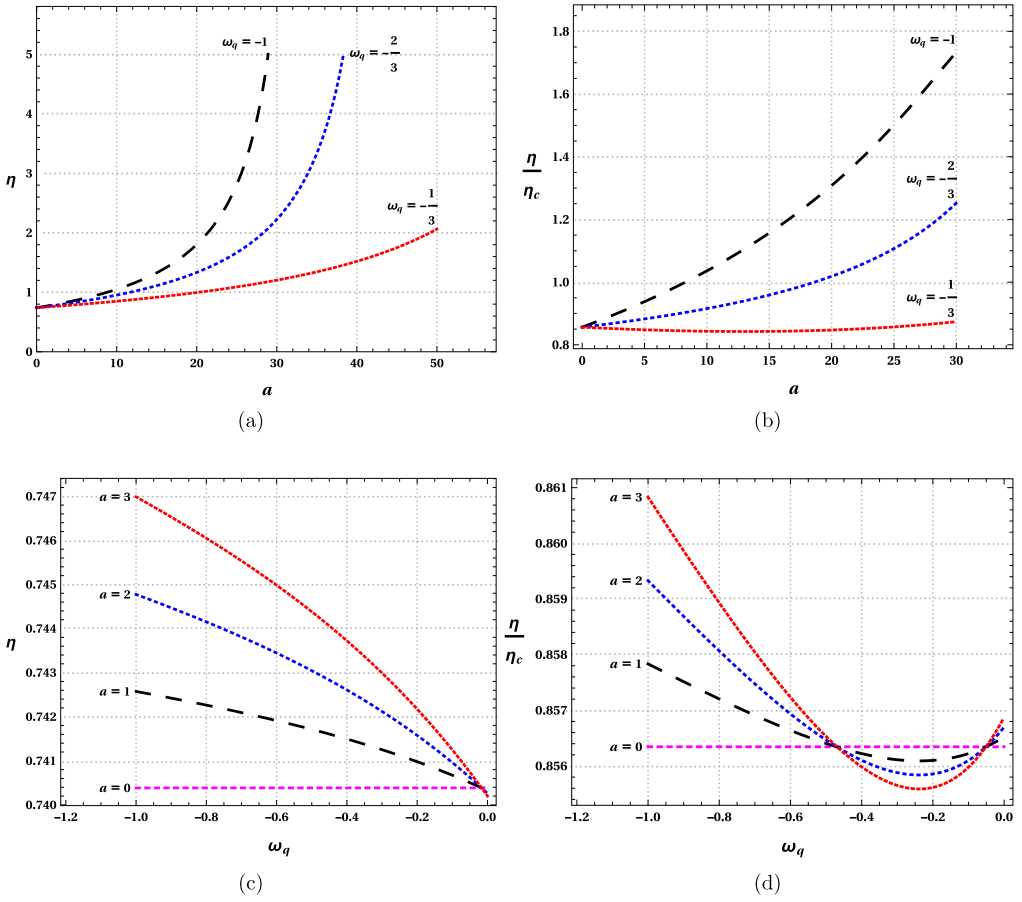

Fig. 7. *The effect of quintessence on the efficiency η of the engine and on the ratio η/η_c with different variables.* In the Figs. 7(a) and 7(b) the dependence on a is studied with different values of ω_q. Here we take $P_1 = 4$, $P_4 = 1$ $S_1 = 1$, $S_2 = 4$ and $\beta = 0.1$. In the second set of Figs. 7(c) and 7(d) behavior against state parameter ω with different values of a is shown. In this case we take $P_1 = 4$, $P_4 = 1$ $S_1 = 1$, $S_2 = 4$ and $\beta = 0.1$.

of 0.75. This is not surprising result because the quintessence density (ρ_q) decreases with increase in ω_q (29). Then we study the role of pressure P_1 on η and η/η_C with different values of quintessence strength a shown in Fig. 6(e) and 6(f), where the functional appearance remains same. The efficiency and its ratio improve with higher pressures and with quintessence. But it is noticed that there is a faster convergence to limiting value 1 in the quintessence case.

At the final stage of our investigation we focus on the action of quintessence parameter a and ω_q. For all three values of ω_q efficiency increases exponentially, when it is plotted against quintessence constant a (Fig. 7(a)). The scenario remains same for the ratio plot, with an exception at $\omega_q = -1/3$, which has a slight decaying nature initially (Fig. 7(b)). We note that in these two plots the efficiency shoots over unity which is a clear violation of second law of thermodynamics. To avoid this unphysical situation we must be careful enough to choose quintessence parameters. In Fig. 7(c) and 7(d), we present the effect of ω_q on η and η/η_C for different values of a. In the light of earlier point, quintessence density (ρ_q) decreases with increasing ω_q, the ef-

Table 1
Deviation in heat engine efficiency η, with variation of quintessence equation of state parameter ω_q and strength parameter a.

a	ω_q	η	a	ω_q	η
1	$-1/3$	0.800	3	$-1/3$	0.804
1	$-2/3$	0.809	3	$-2/3$	0.833
1	-1	0.817	3	-1	0.859

ficiency is higher for smaller values of ω_q. This inference is drawn by considering the physically meaningful range $-1 < \omega_q < -1/3$.

The effect of quintessence on the efficiency of regular black hole heat engine is summarized in the Table 1.

5. Conclusions and discussions

Regular black holes are of great interest in physics as they do not possess singularity. In this article, we demonstrated that the regular Bardeen AdS black hole can be used as an engine to extract energy. The efficiency of the engine is improved by immersing the black hole system in a quintessential field, which has the motivations from cosmology where quintessence can be interpreted as a candidate for dark energy.

In the first part of the article we investigated the thermodynamics of the black hole in the extended phase space. The black hole exhibits a first order phase transition between a small black hole (SBH) phase and a long black hole (LBH) phase, with features similar to that of conventional van der Waals fluid. The critical behavior of the black hole is studied from isotherms and the isobars in the $P - v$ and $T - S$ planes, respectively. The phase transition properties are also drawn from the specific heat study. The diverging nature of specific heat C_P, below the critical point, reflects the first order transition of the black hole.

In the second part of the article, we constructed a heat engine by taking the regular Bardeen black hole as working substance. A cycle in $P - V$ plane is assigned for the black hole with two isotherms and isochores. The efficiency of the engine is calculated by using the work done and heat absorbed during the cycle. As it is customary to compare the efficiency of any engine with Carnot engine, we have compared our results with the corresponding Carnot efficiency. Detailed analysis of the dependence of efficiency η on S_2 (entropy of LBH phase), P_1 (pressure in SBH phase) and β (monopole charge) are done. Among the several observations, we emphasize that the increase in entropy difference between SBH phase (S_1) and LBH phase (S_2) increases the efficiency of the engine. We have made a successful attempt to improve the efficiency of engine by adding a quintessence field. The heat engine efficiency depends on the quintessence parameters ω_q and a. We have presented detailed discussion on the improvement of engine efficiency with quintessence parameters. The quintessence parameter a increases the efficiency and ω_q decreases the efficiency η. We observed a drop in the efficiency η in the quintessence range $-1 < \omega_q < -1/3$. This happens because quintessence matter density (ρ_q) decreases with increase in ω_q value. It is worth mentioning that accelerated expansion of universe takes place in this quintessence range of ω_q. And in this range, the presence of quintessence matter around the black hole improves the efficiency of heat engine. The effect of intensity of quintessential matter field on the heat engine efficiency of regular black hole underlines the importance of quintessence in black hole thermodynamics. This result is promising, when one considers the quintessence as

a viable model for dark energy. We expect that our study in this regard will shed light on the thermodynamics of quintessential AdS black holes.

CRediT authorship contribution statement

Rajani K.V.: Methodology, Software, Visualization, Investigation, Writing - Original draft preparation, **Ahmed Rizwan C.L.**: Software, Formal analysis, Visualization, Investigation, Writing - Original draft preparation, **Naveena Kumara A.**: Software, Data curation, Formal analysis, Visualization, Investigation, Writing - Original draft preparation, **Deepak Vaid**: Conceptualization and Supervision, **Ajith K.M.**: Conceptualization and Supervision.

Declaration of competing interest

The authors declare that they have no known competing financial interests or personal relationships that could have appeared to influence the work reported in this paper.

Acknowledgements

The authors R.K.V., A.R.C.L. and N.K.A. would like to thank the department of physics, National Institute of Technology Karnataka. The authors A.R.C.L. and N.K.A. also thank UGC, Govt. of India for financial support through SRF scheme.

References

[1] J.D. Bekenstein, Lett. Nuovo Cimento (1971–1985) 4 (1972) 5.
[2] J.D. Bekenstein, Phys. Rev. D 7 (8) (1973) 2333.
[3] J.D. Bekenstein, Phys. Rev. D 9 (12) (1974) 3292.
[4] S.W. Hawking, Commun. Math. Phys. 43 (3) (1975) 199.
[5] J.M. Bardeen, B. Carter, S.W. Hawking, Commun. Math. Phys. 31 (2) (1973) 161.
[6] S.W. Hawking, D.N. Page, Commun. Math. Phys. 87 (4) (1983) 577.
[7] J. Maldacena, Int. J. Theor. Phys. 38 (4) (1999).
[8] E. Witten, Adv. Theor. Math. Phys. 2 (1998) 505.
[9] A. Chamblin, R. Emparan, C.V. Johnson, R.C. Myers, Phys. Rev. D 60 (1999) 064018.
[10] A. Chamblin, R. Emparan, C.V. Johnson, R.C. Myers, Phys. Rev. D 60 (1999) 104026.
[11] M.M. Caldarelli, G. Cognola, D. Klemm, Class. Quantum Gravity 17 (2) (2000) 399.
[12] D. Kastor, S. Ray, J. Traschen, Class. Quantum Gravity 26 (19) (2009) 195011.
[13] C. Teitelboim, Phys. Lett. B 158 (4) (1985) 293.
[14] J.D. Brown, C. Teitelboim, Nucl. Phys. B 297 (4) (1988) 787.
[15] B.P Dolan, Class. Quantum Gravity 28 (12) (2011) 125020.
[16] B.P Dolan, Class. Quantum Gravity 28 (23) (2011) 235017.
[17] D. Kubizňák, R.B. Mann, J. High Energy Phys. 2012 (7) (2012) 33.
[18] S. Gunasekaran, D. Kubizňák, R.B. Mann, J. High Energy Phys. 2012 (11) (2012) 110.
[19] A. Belhaj, M. Chabab, H. El Moumni, M.B. Sedra, Chin. Phys. Lett. 29 (10) (2012) 100401.
[20] N. Altamirano, D. Kubizňák, R.B. Mann, Phys. Rev. D 88 (2013) 101502.
[21] R. Zhao, H.H. Zhao, M.S. Ma, L.C. Zhang, Eur. Phys. J. C 73 (12) (2013) 2645.
[22] S.H. Hendi, M.H. Vahidinia, Phys. Rev. D 88 (2013) 084045.
[23] C. Song-Bai, L. Xiao-Fang, L. Chang-Qing, Chin. Phys. Lett. 30 (6) (2013) 060401.
[24] E. Spallucci, A. Smailagic, Phys. Lett. B 723 (4) (2013) 436.
[25] A. Belhaj, M. Chabab, El Moumni, K. Masmar, M.B. Sedra, A. Segui, J. High Energy Phys. 2015 (5) (2015) 149.
[26] H.F. Li, H.H. Zhao, L.C. Zhang, R. Zhao, Eur. Phys. J. C 77 (5) (2017) 295.
[27] L.C. Zhang, H.H. Zhao, R. Zhao, M.S. Ma, Adv. High Energy Phys. 7 (2014) 816728.
[28] H.H. Zhao, L.C. Zhang, M.S. Ma, R. Zhao, Class. Quantum Gravity 32 (14) (2015) 145007.

[29] O. Ökcü, E. Aydıner, Eur. Phys. J. C 77 (2017).
[30] C.L. Ahmed Rizwan, A. Naveena Kumara, D. Vaid, K.M. Ajith, Int. J. Mod. Phys. A 33 (35) (2018) 1850210.
[31] C.V. Johnson, Class. Quantum Gravity 31 (20) (2014) 205002.
[32] A. Chakraborty, C.V. Johnson, Int. J. Mod. Phys. D 27 (16) (2018) 1950012.
[33] C.V. Johnson, Entropy 18 (4) (2016) 120.
[34] R. Penrose, Nuovo Cimento Riv. Ser. 1 (1969).
[35] T. Piran, J. Shaham, J. Katz, Astrophys. J. Lett. 196 (1975) L107.
[36] K. Jafarzade, J. Sadeghi, Int. J. Theor. Phys. 56 (11) (2017) 3387.
[37] M.R. Setare, H. Adami, Phys. Rev. D 91 (2015) 084014.
[38] C.V. Johnson, Class. Quantum Gravity 33 (13) (2016) 135001.
[39] M. Zhang, W.B. Liu, Int. J. Theor. Phys. 55 (12) (2016) 5136.
[40] C.V. Johnson, Class. Quantum Gravity 33 (21) (2016) 215009.
[41] S.W. Wei, Y.X. Liu, arXiv:1708.08176, 2017.
[42] J.X. Mo, G.Q. Li, J. High Energy Phys. 2018 (5) (2018) 122.
[43] S.H. Hendi, B.E. Panah, S. Panahiyan, H. Liu, X.H. Meng, Phys. Lett. B 781 (2018) 40.
[44] H. Xu, Y. Sun, L. Zhao, Int. J. Mod. Phys. D 26 (13) (2017) 1750151.
[45] J.X. Mo, F. Liang, G.Q. Li, J. High Energy Phys. 2017 (3) (2017) 10.
[46] R.A. Hennigar, F. McCarthy, A. Ballon, R.B. Mann, Class. Quantum Gravity 34 (17) (2017) 175005.
[47] J. Zhang, Y. Li, H. Yu, Eur. Phys. J. C 78 (8) (2018) 645.
[48] H. Liu, X.H Meng, Eur. Phys. J. C 77 (8) (2017) 556.
[49] J.M. Bardeen, in: Proc. Int. Conf. GR5, Tbilisi, vol. 174, 1968.
[50] E. Ayon-Beato, A. Garcia, Phys. Rev. Lett. 80 (1998) 5056.
[51] S.A. Hayward, Phys. Rev. Lett. 96 (2006) 031103.
[52] M. Akbar, N. Salem, S.A. Hussein, Chin. Phys. Lett. 29 (7) (2012) 070401.
[53] C.L. Ahmed Rizwan, A. Naveena Kumara, K.V. Rajani, D. Vaid, K.M. Ajith, arXiv:1811.10838, 2018.
[54] A.G. Tzikas, Phys. Lett. B 788 (2019) 219.
[55] E. Ayon-Beato, A. Garcia, Phys. Lett. B 493 (1) (2000) 149.
[56] V.V. Kiselev, Class. Quantum Gravity 20 (6) (2003) 1187.
[57] S. Tsujikawa, Class. Quantum Gravity 30 (21) (2013) 214003.
[58] S. Chen, Q. Pan, J. Jing, Class. Quantum Gravity 30 (14) (2013) 145001.
[59] S. Chen, J. Jing, Class. Quantum Gravity 22 (4) (2005) 4651.
[60] G.Q. Li, Phys. Lett. B 735 (4) (2014) 256.
[61] Z.Y. Fan, Eur. Phys. J. C 77 (4) (2017) 266.
[62] M. Saleh, B.B. Thomas, T.C. Kofane, Int. J. Theor. Phys. 57 (9) (2018) 2640.
[63] B.B. Thomas, M. Saleh, T.C. Kofane, Gen. Relativ. Gravit. 44 (9) (2012) 2181.
[64] W. Yi-Huan, C. Zhong-Hui, Chin. Phys. Lett. 28 (10) (2011) 100403.
[65] K.K.J. Rodrigue, M. Saleh, B.B. Thomas, T.C. Kofane, arXiv:1808.03474, 2018.